ACS OMEGA

Open Access

http://pubs.acs.org/journal/acsodf

Article

Zinc Oxide Nanoparticles: Applications in Photocatalysis of Dyes and Pearl Millet Seed Priming for Enhanced Agricultural Output

Rajesh Kumar, Irra Dhar, and Madan Mohan Sharma*

Cite This: *ACS Omega* 2025, 10, 7181−7193

Read Online

ACCESS | Metrics & More | Article Recommendations

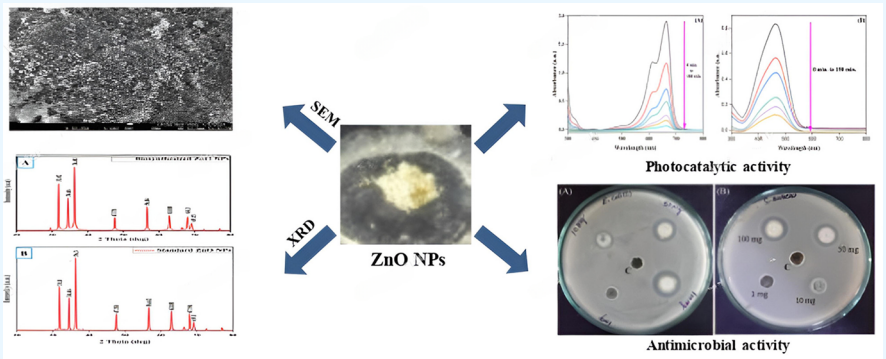

ABSTRACT: This research examines the environmentally benign manufacture of zinc oxide nanoparticles employing a crude extract from *Murraya koenigii* leaves as a capping and reducing agent. The considerable peak of synthesized zinc oxide nanoparticles (ZnO NPs) was observed at 335 nm, and the functional groups of plant active metabolites to reduce zinc and evaluate shape and elemental compositions were analyzed using UV−vis spectroscopy, FT-IR, SEM, and EDX analysis, respectively. The average size of synthesized zinc oxide nanoparticles (27.26 nm) was validated by XRD using the Debye−Scherrer's equation. Zinc oxide nanoparticles were assessed for their efficiency in seed priming, photocatalytic degradation, antibacterial activity, and antioxidant abilities. The biosynthesized zinc oxide nanoparticles were utilized in seed priming, significantly enhancing germination rate (90%), shoot length (5.46 cm), and root length (15.13 cm) at a concentration of 150 ppm in comparison to control. Further, the effect of methyl orange (MO) and methylene blue (MB) dyes on % seed germination and plant growth of hybrid pearl millet was studied *in vitro*. MO and MB had shown approximately 15 and 46% reduction in seed germination % in comparison to control. Additionally, zinc oxide nanoparticles had shown remarkable photocatalytic degradation of 94.45% against methylene blue and 85.99% against methyl orange. Zinc oxide nanoparticles were also effective against *Escherichia coli* and *Staphylococcus aureus* bacteria, with zones of inhibition of 0.45 and 0.35 cm at a 100 mg/mL concentration. Furthermore, zinc nanoparticles observed higher antioxidant activity against DPPH at 80 μg/mL. The present finding highlights the potential of biosynthesized zinc oxide nanoparticles as a sustainable approach to agriculture, environmental remediation, and biological sciences.

1. INTRODUCTION

Nanotechnology has a promising avenue for the synthesis of nanoparticles, particularly due to its environmentally friendly and sustainable attributes. Owing to their unique features, zinc nanoparticles have received attention, including huge surface area, excellent stability, and a unique electrical structure. These characteristics make zinc oxide nanoparticles highly effective in photocatalysis. The various dyes used in the decoctions are toxic and nonbiodegradable, which pollutes water bodies, blocks light from entering the environment, and reduces soil productivity. The high amounts of dangerous and resistant compounds discovered in textile-based industrial effluent dyes are largely caused by the global textile industries.[1] Sugar and textile industry effluents at pH 7.1−9.1 and 8.1−9.1 have been shown to negatively impact soil microorganisms.[2] Textile dye effluent decreased water's dissolved oxygen content and populations of aquatic microbes have also been found to be negatively affected by azo dyes.[3,4] Azo dyes can harm soil's chemical and biological qualities, threatening agricultural output and food security.[5] The quality of groundwater is severely negatively impacted by untreated hazardous wastewater.[6] These harmful substances (dyes) accumulated in living

Received: November 22, 2024
Revised: January 9, 2025
Accepted: January 16, 2025
Published: February 14, 2025

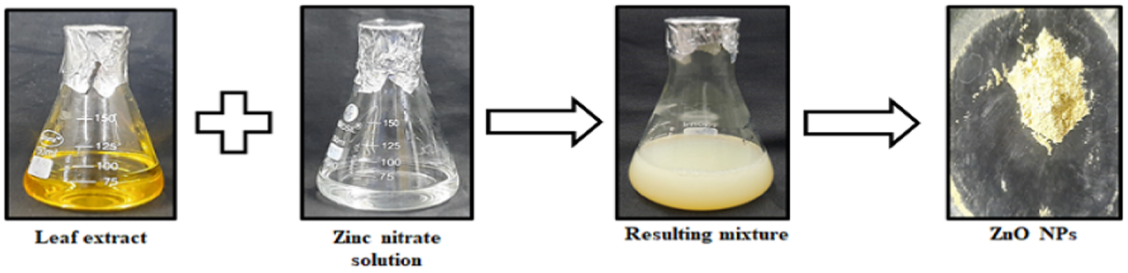

Figure 1. Biosynthesis of zinc oxide nanoparticles using *Murraya koinigii* dry leaf extract.

cells, reduced cell activity, slowed down growth, and resulted in a number of deficiencies and illnesses.[7,8] Whereas, the phytotoxic effect of MO and MB dyes was shown on wheat[9] and *Cicer arietinum*.[10] Reduced seed germination and other aspects of plant growth are the effects of these dyes on agricultural crops. Additionally, reports have indicated that crops like, Country beans,[11] lady finger,[12] and red amaranth[13] are evaluated using high dyeing industry effluent, which results in decreased seed germination and plant growth. The development of seedlings is negatively impacted by the existence of toxic metals and other detrimental chemicals.[14] In contrast, zinc (Zn), an essential micronutrient, plays a pivotal role in maintaining cellular homeostasis and supporting various biological functions. Zinc is present in several kinds of enzymes, including hydrolases, transferases, ligases, oxidoreductases, and isomerases.[15] It participates in a variety of functions, including disease resistance, photosynthesis, and the antioxidant defense system.[10−13] Zinc has recently been employed as zinc oxide nanoparticles, which have been reported for enhanced seed germination, destroyed organic agricultural commodities' photocatalytic process, and antibacterial activity.[16−18] The synthesized zinc oxide nanoparticles reported the highest germination rates (1.25 μg/mL) of okra seeds, as well as the longest shoot and root lengths (1 μg/mL).[19] Methylene blue, Congo red, and methyl orange are three azo dyes that were found to photodegrade 91, 97, and 85% after 120 min of being exposed to sunlight through biosynthesized nanocomposite.[20] Apart from zinc nanoparticles, the synthesis of Au nanoparticles demonstrated 80% effectiveness in degrading MB dye in 90 min and FALE@Au nanoparticles showed strong photocatalytic activity (80%) efficiency against both methyl orange and methylene blue dyes.[21,22] Zinc oxide nanoparticles have an effective electrical structure and are safe for the environment and nontoxic, and they are frequently utilized in photocatalytic degradation.[23,24] Whereas, photocatalytic degradation % through zinc nanoparticles was also reported in methyl orange[25] and methylene blue.[26]

The germination of seeds is a significant issue in the vicinity of industrial locations, where various dyes are discharged into agricultural land. This study presents the biological production of zinc oxide nanoparticles and assesses their efficacy in promoting seed germination and photocatalytic degradation activity against methylene blue (MB) and methyl orange (MO) dyes. Additionally, produced zinc nanoparticles were examined for both antibacterial and antioxidant properties. Zinc oxide nanoparticles that have been biosynthesized show great promise for environmental remediation, especially when it comes to breaking down dangerous dyes and encouraging environmentally friendly behaviors in a variety of sectors.

2. MATERIALS AND METHODS

2.1. Materials Required. Reagents, methyl orange (MO), methanol, methylene blue (MB), DPPH (2,2-diphenyl-1-picrylhydrazyl), and nutrient agar were purchased from Himedia. Cultures of *Staphylococcus aureus* (MTCC 96) and *Escherichia coli* (MTCC 1652) were procured from the Institution of Microbiology (IMTECH), Chandigarh, India. Reagents, sodium hydroxide (NaOH), and zinc nitrate hexahydrate [$Zn(NO_3)_2.6H_2O$] were from E-Merck. Milli-Q water was used for the entire experiment. ZnO NPs (used as a standard) was purchased from Sigma-Aldrich. Pearl millet (HHB-67 improved) seeds were procured from the Rajasthan Agriculture Research Institute (RARI), Durgapura, Jaipur, India.

2.2. Aqueous Leaf Extract Preparation. *Murraya koinigii* leaves were taken from the Manipal University Jaipur (MUJ) campus in Jaipur, Rajasthan, India, in January 2024. The collected leaf samples were thoroughly cleaned with ultrapure water to remove any impurities such as dust or debris. After cleaning, the leaves were carefully cut into small pieces to facilitate uniform drying. The leaf samples were subjected to drying in a hot air oven at 50 °C for 48 h to ensure total moisture removal. The desiccated leaves, now fragile, were further pulverized with a mortar and pestle. 10 g of powdered leaves were combined with 100 mL of Milli-Q water and boiled in a water bath at 70 °C for 30 min. Upon reaching room temperature, the mixture was subjected to filtration with Whatman No. 1 filter paper. The filtrate was stored at 4 °C until needed.

2.3. Zinc Oxide Nanoparticles Biosynthesis. A 50 mL solution of 0.1 M zinc nitrate hexahydrate [$Zn(NO_3)_2{\cdot}6H_2O$] was mixed with 10 mL of *Murraya koenigii* leaf extract and subjected to a magnetic stirrer for comprehensive mixing. After 6 h, 1 M (50 mL) NaOH solution was put in the reaction mixture, and then the mixture was stirred at 60 °C overnight (Figure 1).

The combination changed to a creamy white. The white mixture was then spun at 8000 rpm for 20 min. Following washing with ethanol, the precipitate was rinsed at least three times with Milli-Q water. The white solid was then dehydrated in a hot air oven before being pounded into a fine powder with a ceramic mortar and pestle (Figure 1). Subsequently, the fine powder was examined using UV−vis (UV−visible spectroscopy), FT-IR (Fourier transform infrared spectroscopy), EDS (energy-dispersive X-ray spectroscopy), SEM (scanning electron microscopy), and XRD (X-ray diffraction). The process by which ZnO NPs were biosynthesized using several equations:

$$Zn(NO_3)_2 \leftrightarrow Zn^{2+} + 2NO_3^- \quad (1)$$

https://doi.org/10.1021/acsomega.4c10628
ACS Omega 2025, 10, 7181−7193

$$H_2O \leftrightarrow H^+ + OH^- \quad (2)$$

$$NaOH \leftrightarrow Na^+ + OH^- \quad (3)$$

In the mixture of reactants, zinc nitrate ($Zn(NO_3)_2$ breaks down into zinc ions (Zn^{2+}) and nitrate ions ($2NO_3^-$) (eq 1), the molecules of water decompose into hydroxyl and hydrogen ions (eq 2), and sodium hydroxide, which serves as a strong basic, divides into Na+ (sodium) and hydroxyl (OH) ions (eq 3).

$$Zn^{2+} + 4OH^- \leftrightarrow [Zn(OH)_4]^{2-} \quad (4)$$

$$2[Zn(OH)_4]^{2-} \rightarrow 2ZnO + 4H_2 + 3O_2 \quad (5)$$

In an alkaline mixture, zinc ions (Zn^{2+}) combine via hydroxide ions (OH^-) to form a steady zinc hydroxide complex $[Zn(OH)_4]^{2-}$ (eq 4). The zinc hydroxyl complex decomposes under external energy, such as ultrasonic exposure to radiation, producing zinc oxide and releasing hydrogen (H_2) and oxygen (O_2) gases (eq 5).[27] There are several biochemical compounds (alkaloid, phenol, and flavonoid) present in the extracts of murraya leaves. Different functional groups of these compounds were in charge of reducing zinc to zinc oxide.[31,45,46]

2.4. Characterization of Zinc Oxide Nanoparticles. *2.4.1. UV−Visible Spectroscopy.* The ultraviolet−visible spectroscopy technique was utilized to perform the preliminary characterization of zinc oxide nanoparticles. For 20 min, the solution of ZnO NPs (1 mg) and Milli-Q water (1 mL) was sonicated. The sonicated zinc oxide nanoparticle (10 times diluted) solution's spectrum was analyzed between 200 and 600 nm (Shimadzu UV-2600, MUJ).

2.4.2. Fourier Transform Infrared Spectroscopy. FT-IR technique is used for identifying and characterizing organic and inorganic materials based on their interaction with infrared (IR) light. A trustworthy scientific method for determining functional groups is Fourier transform infrared spectra analysis. An examination of the infrared absorption spectra reveals the numerous bonds that are present in the zinc oxide nanoparticles that were manufactured (Model-Bruker Alpha, MUJ).

2.4.3. Scanning Electron Microscopy and Energy-Dispersive Spectrometry. A three-dimensional image of the morphology of nanomaterials can be obtained using a scanning electron microscope. It is utilized for the purpose of examining the external morphology of zinc oxide nanoparticles that have been synthesized. To conduct the FESEM examination, fine powder formed from zinc oxide nanoparticles was utilized, which was performed using the JSM-7610 F-Plus microscope at MUJ. For EDS, the same materials and equipment were used. Zinc oxide NP's elemental composition is analyzed qualitatively and quantitatively using EDS.

2.4.4. X-ray Diffraction. The crystalline structure and average size of the produced zinc oxide nanoparticles are revealed by X-ray diffraction. To determine whether the zinc oxide nanoparticles made by SMART LAB (MUJ) were crystalline, the 2θ scanning range was adjusted between 20° and 80°. The produced zinc oxide nanoparticles' average crystallographic size was determined by applying the Debye−Scherrer formula:

$$D = 0.9\lambda/\beta \cos\theta$$

where D is the average crystal size of zinc oxide nanoparticles, β is the full width at half-maximum of the diffraction peak, λ is the wavelength, and θ is the diffraction angle.

2.4.5. ζ-Potential. A measurement of the stability in suspension (solution) was carried out with the help of ζ-potential. Utilizing a ζ-potential device (Anton Paar Litesizer 500), the zinc oxide nanoparticles that were produced through biosynthesis were determined. As a foundation for determining the ζ-potential, the trend and velocity of nanoparticles in response to the action of a known electric field are utilized.

2.4.6. TGA (Thermogravimetric Analysis). To determine the heat stability, composition, and phase shifting, zinc oxide nanoparticles are subjected to thermogravimetric analysis (Shimadzu DTG-60H). Thermogravimetric analysis (TGA) was conducted to examine the thermal stability and decomposition characteristics of zinc oxide nanoparticles produced from the murraya leaf extract. Stability testing was conducted using the fine powder from room temperature up to 1000 °C.

2.5. Seed Germination Test. A solution of MO and MB dyes was produced to examine seed germination. Four different concentrations (0.5, 1, 1.5, and 2%) of both dyes were prepared. The seeds of pearl millet were sterilized with sodium hypochlorite (0.1%) for 2 min and then rinsed thrice with Milli-Q water to eliminate chloride ions. The experiment of seed germination was conducted through the paper towel method in petriplates. Twenty seeds were placed in each petriplate and treated with prepared different concentrations (0.5−2%) of dye solution. Separately, a 5 mL solution of each dye was added to each plate. In contrast, a priming test using the same category of pearl millet seed was carried out using different amounts of plant-mediated zinc oxide nanoparticles (50, 100, 150, and 200 ppm). All petriplates were incubated at ambient temperature (28 ± 2 °C) for 5 days in a plant growth chamber. After incubation for 5 days, germination % and other physiological parameters (shoot length and root length) of 20 random plants of each set-up pearl millet seedlings were recorded:

$$\text{germination percentage (GP)} = \text{seeds germinated/total seeds} \times 100$$

2.6. Photocatalytic Degradation. *2.6.1. Methylene Blue.* With minor modifications, MB degradation in ultraviolet (UV) light was used to assess the photodegradation responses of produced ZnO NPs.[28] In the beginning, a conical flask with a capacity of 250 mL was used to prepare 100 mL of an MB solution with a concentration of 20 ppm. After dispersing 10 mg of zinc oxide nanoparticle powder in MB, the mixture was put into a sonicator for 10 min. Next, the mixture was exposed to UV radiation for 30, 60, 90, 120, 150, and 180 min at various intervals. After centrifugation at 8000 rpm (10 min), the reactivity of effluent was measured in a UV−visible spectrophotometer at 663 nm.

2.6.2. Methyl Orange. The photocatalytic degradation was determined by zinc oxide nanoparticles by employing UV light to examine the breakdown of MO dye. 20 ppm (100 mL) solution was made of methyl orange and 10 mg of zinc oxide nanoparticles (photocatalyst) were added to the solution of methyl orange. To mix the solution of photocatalyst and MO, both were placed on a shaker incubator in the dark for 1 h to evaluate the desorption-adsorption equilibrium. After that, the resulting solution was exposed to UV light for photocatalytic

https://doi.org/10.1021/acsomega.4c10628
ACS Omega 2025, 10, 7181−7193

reaction. To remove the photocatalyst, 10 min was spent centrifuging the reaction mixture at 8000 rpm. After that, at various time differences (30, 60, 90, 120, and 150 min), the absorbance was taken of clear solution at 464 nm through a UV−visible spectrophotometer.

MB/MO dye degradation % was determined by the following equation:

$$\text{degradation (\%)} = [(A_0 - A)/A_0] \times 100$$

where A_0 = initial absorption of MB/MO dye and A = absorption of the resulting mixture after UV light exposure.

2.7. Antibacterial Assay. The antibacterial assay was performed by well diffusion method against *S. aureus* and *E. coli*.[29] Milli-Q water was utilized as a negative control (designated by C), and the zinc oxide nanoparticle (sample) was inoculated in different quantities (1, 10, 50, and 100 mg/mL). Each petriplate well contained a 50 μL sample. Following sample loading, the petriplates were incubated for 24 h at 37 °C. A measuring scale was utilized to ascertain the zone of inhibition.

2.8. Antioxidant Assay. The synthesized zinc nanoparticles were tested against DPPH with slight modification.[30] At different concentrations (10 and 80 μg/mL), aliquots of the extracted material (samples) were incorporated into 0.1 mM DPPH methanolic solutions. The reaction mixture was thereafter kept for 30 min in darkness at ambient temperature. The optical density (OD) of the resultant mixture was assessed by UV−visible spectroscopy at 517 nm. Ascorbic acid was used as control for this experiment. The subsequent formula was employed to calculate the % inhibition:

$$\text{inhibition (\%)} = \frac{\text{absorbance of control} - \text{absorbance of sample}}{\text{absorbance of control}} \times 100$$

2.9. Statistical Analysis. Most of the experiments were carried out in laboratories with mean ± standard deviation (SD) in triplicates. Data on mechanical characteristics were subjected to ANOVA analysis using SPSS (IBM, SPSS Statistical software, 29.0). The p-value was less than 0.05, and the differences were confirmed using Duncan's test.

3. RESULTS AND DISCUSSION

Zinc oxide nanoparticles were successfully synthesized utilizing Murraya dry leaf extract, and their characteristics were described. The amount of leaf extract must be sufficient to ensure the availability of the bioactive ingredient, which will enable effective stabilization and nanoparticle reduction. In this investigation, 10 mL of leaf extract was utilized for the manufacture of zinc nanoparticles. There are numerous studies indicating that 10 mL of plant extract was sufficient for reducing the zinc ion.[31,32] The synthesized zinc oxide nanoparticles demonstrated antioxidant and photocatalytic degradation potential uses as well as the environmental effects of dye toxicity on seed germination.

3.1. pH Analysis. The pH analyses of the different components in the reaction mixture are shown (Table 1).

3.2. UV−Vis Spectroscopy Analysis. Ultraviolet−visible spectroscopy was utilized to carry out early characterization of zinc oxide nanoparticles that were produced through biosynthesis. The sonicated sample of zinc oxide nanoparticles was placed between the light source and photodetector and the peak was observed at 335 nm (Figure 2).

Table 1. Analyzed pH Reactants

components	pH
50 mL of $Zn(NO_3)_2{\cdot}6H_2O$ (0.1 M)	5.67
Murraya dry leaf extract	5.46
1 M NaOH (50 mL)	14.20
leaf extract + NaOH + $Zn(NO_3)_2$	13.73

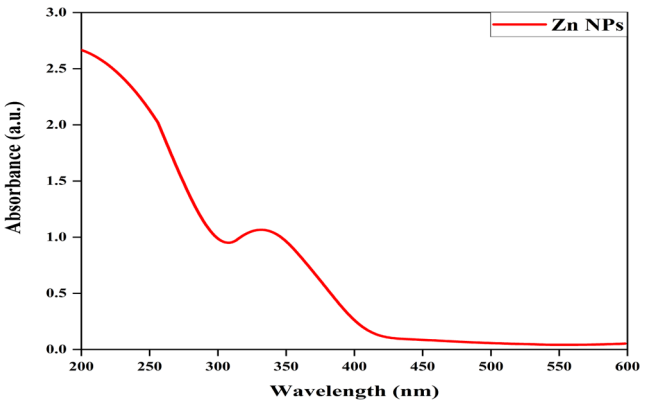

Figure 2. Biosynthesized zinc oxide nanoparticles' UV−visible spectrum.

This peak indicates that biosynthesized zinc oxide nanoparticles absorb light at a particular wavelength. Our findings are consistent with previously published articles of synthesized zinc oxide nanoparticles through callus extract of *Ziziphus spina-cristi* and leaf extract of *Cassia alata*.[33,34] Biosynthesized zinc oxide nanoparticles derived from the seed of *Nigella sativa* L. showed a peak at 230 nm,[35] which differs from our findings. This variation may be attributed to different experimental conditions, methods, and materials.

3.3. FT-IR Analysis. Murraya leaf extract was used to find functional groups that reduce and cap zinc oxide nanoparticles using FT-IR. Significant peaks in the spectra of normal zinc oxide, plant-derived extract, and biosynthesized zinc oxide nanoparticles indicate essential functional entities that participate in the chemical reaction process (Figure 3).

The Murraya leaf extract spectrum displayed prominent peaks corresponding to O−H stretching vibrations at 3850, 3742, and 3220 cm^{-1}, attributed to phenols and alcohols, indicating their potential role as reducing agents.[36,37] The peaks at 2353 cm^{-1} (C−O stretching), 1518 cm^{-1} (O═C═O

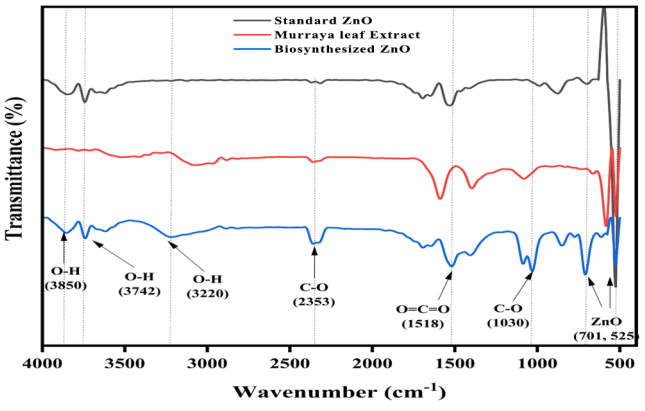

Figure 3. FT-IR spectrum of standard zinc oxide, Murraya leaf extract, and biosynthesized zinc oxide nanoparticles.

https://doi.org/10.1021/acsomega.4c10628
ACS Omega 2025, 10, 7181−7193

stretching), and 1030 cm^{-1} (C−O stretching) represent characteristic functional groups of organic compounds that may contribute to nanoparticle stabilization (Table 2).[38,39]

Table 2. Different Functional Groups Involved in the Biosynthesis of Zinc Oxide Nanoparticles Represent Various Wavenumbers

wavenumber (cm^{-1})	functional group	assignment
3850, 3742, 3220	O−H	hydroxyl group
2353, 1030	C−O	alcohol and ester group
1518	O═C═O	carbonyl group
701, 525	Zn−O	zinc oxide

The spectra of zinc oxide nanoparticles had analogous peaks with slight variations in their locations and intensities, suggesting the participation of functional components from the plant aqueous leaf extract in relationships with the nanoparticle surface. The existence of a significant band at 525 cm^{-1} validated the Zn−O stretching vibrations, signifying the successful synthesis of zinc oxide nanoparticles. The stretching vibrations of metal−oxide (M−O) bonds were detected in the hallmark range between 400 and 700 cm^{-1}.[40−42] The resemblance among peak frequencies of the biosynthesized zinc oxide nanoparticles and those of ordinary zinc oxide verified that the biosynthesized nanoparticles were generated successfully with analogous properties. The bonding of several other nanoparticles, such as Ag nanoparticles, was supported by the bands at 525 cm^{-1} in the FT-IR spectra.[43,44] The unidentified peaks in the murraya leaf extract's FT-IR spectra are thought to have no role in capping and reducing agents.

3.4. FESEM and EDS Analysis. The morphology of biosynthesized zinc oxide nanoparticles was revealed by FESEM. The picture shows zinc nanoparticles with different aggregates (Figure 4).

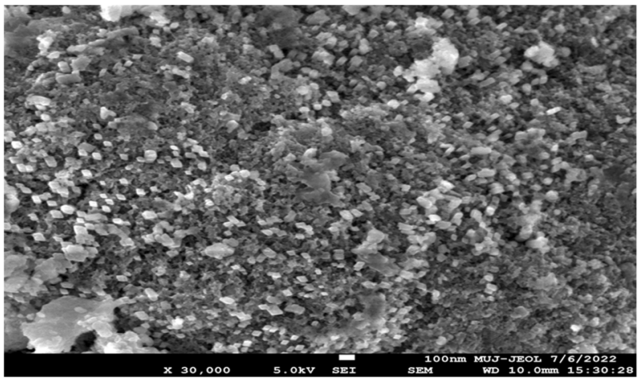

Figure 4. SEM picture of zinc oxide nanoparticles synthesized biologically.

The fine powder was used to characterize the zinc oxide nanoparticles. The biosynthesized zinc oxide nanoparticles were observed to have a spherical shape and were predominantly present in clustered formations. This clustering of nanoparticles can be attributed to various factors, including synthesis conditions, surface properties, and interparticle interactions. The synthesized zinc oxide nanoparticles were consistent with those already reported.[47,48]

EDS spectra showed element detection. The standard ZnO and synthesized zinc nanoparticles were in zinc oxide form due to the presence of Zn (zinc) and O (oxygen) (Figure 5).

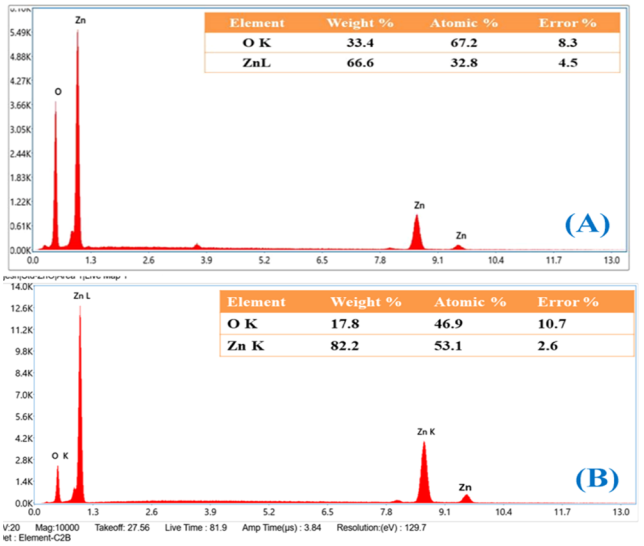

Figure 5. EDS graph and elemental composition table of (A) biosynthesized zinc oxide nanoparticles and (B) standard zinc oxide.

The EDS graph displayed three peaks corresponding to zinc and one peak corresponding to oxygen. One peak of zinc and two peaks of oxygen were present between 0 and 1.3, and two additional zinc peaks appeared between 7.8 and 10.4. The peaks of standard and biosynthesized zinc oxide nanoparticles were identical; therefore, our investigation indicated that biosynthesized nanoparticles are present in the form of zinc (Zn) and oxygen (O). The pattern of peaks of zinc and oxygen were similar to the published reports.[31,49]

3.5. X-ray Diffraction Analysis. The dried powder was analyzed using XRD characterization, revealing distinct peaks in the XRD graph at 2θ values of 32.02, 34.66, 36.48, 47.78, 56.84, 63.08, and 68.20°. These peaks corresponded to the diffraction planes (100), (002), (101), (102), (110), (103), and (112), respectively (Figure 6).

The 2θ values of typical (standard) zinc oxide nanoparticles were practically the same as in biosynthesized nanoparticles, indicating that the produced zinc nanoparticles have a highly crystalline nature. The peaks also demonstrated the purity of the biosynthesized nanoparticles. Biosynthesized zinc oxide nanoparticles were found to have an average crystalline size of 27.26 nm. Multiple studies substantiate the application of leaf extracts to forecast the crystalline characteristics of zinc oxide nanomaterials of *Calotropis gigantea* and *Murraya koenigii*.[31,47]

3.6. ζ-Potential. The ζ-potential (ZP) provides insight into the stability and surface charges of biosynthesized zinc oxide nanoparticles (Figure 7).

The zinc oxide nanoparticles have a ζ-potential value of −27.0 mV demonstrating stability. The extract from murraya leaves may contain hydroxyl groups that are more capable of binding to metal ions. As a result, these compounds may coat the zinc nanoparticles to keep them from accumulating and remain charged negatively. The zinc oxide NRs with −13 mV revealed a strong negative charge.[50] Some additional studies were also consistent with our findings regarding the ζ-potential of produced zinc nanoparticles.[51,52]

https://doi.org/10.1021/acsomega.4c10628
ACS Omega 2025, 10, 7181−7193

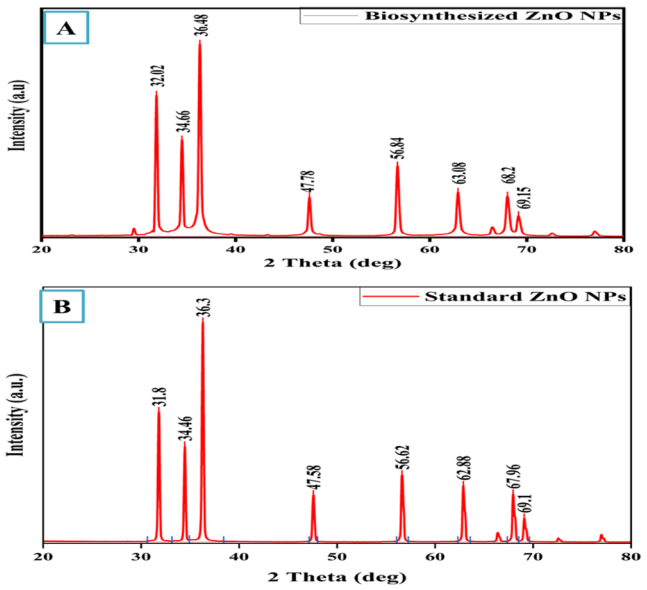

Figure 6. XRD graph of (A) biosynthesized zinc oxide nanoparticles and (B) standard zinc oxide nanoparticles.

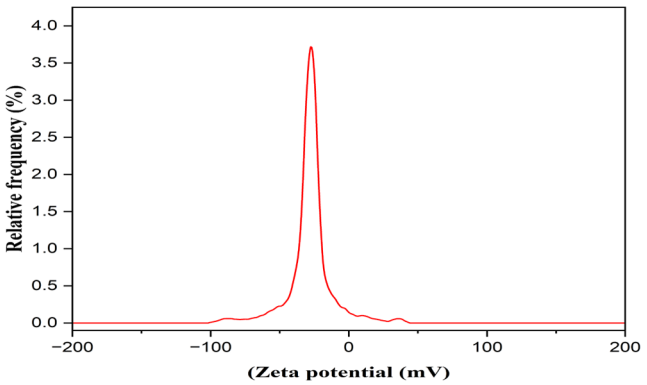

Figure 7. ζ-potential (ZP) graph of biosynthesized zinc oxide nanoparticles.

3.7. TGA (Thermogravimetric Analysis). The TGA curve showed an initial weight loss below 200 °C, which is due to the removal of moisture and contaminants on the nanoparticle surface. A significant weight loss was seen between 200 and 600 °C due to the degradation of organic molecules and volatile employed in the biosynthesis process (Figure 8).

Beyond 600 °C, the weight remained steady, indicating the production of thermally stable zinc oxide nanoparticles. At temperatures exceeding 600 °C, the residual mass was around 70%, indicating that the zinc oxide structure was pure and thermally stable. Thus, the thermograph suggested that biosynthesized zinc oxide nanoparticles are thermally stable, with all volatile and organic components eliminated at increasing temperatures, making them suitable for high-temperature applications.[60−62]

3.8. Band Gap (UV−Vis). The amount of energy necessary for an electron to move through the valence to the conductivity band in the manufactured zinc oxide nanoparticles was measured by examining its absorption by UV−vis spectroscopy (Figure 9).

The TAUC method was used to conduct the band gap investigation. The band gap energy was estimated with eq 6.[53]

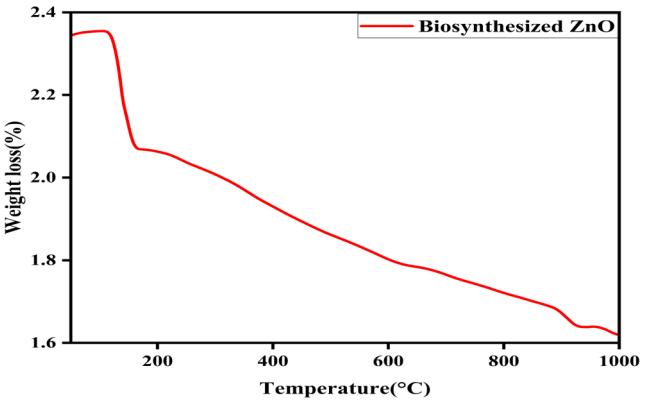

Figure 8. TGA (thermogravimetric analysis) of biosynthesized zinc oxide nanoparticles.

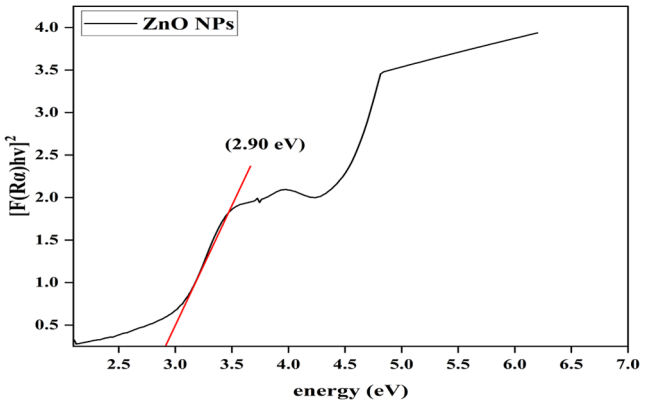

Figure 9. Band gap energy for biosynthesized zinc oxide nanoparticles.

$$\alpha h\nu = A(h\nu - E_g)^{1/2} \quad (6)$$

The spectrum of radiation (UV, visible, or infrared) that zinc oxide nanoparticles can absorb to produce photoinduced pairs of electrons−holes is determined by their band gap. Synthesized zinc nanoparticle has a 2.90 eV band gap (Figure 8). A prominent band gap has the ability to improve photocatalytic degradation. This demonstrates their potential for application in photocatalysis procedures to remove impurities from water. There have been prior reports of similar numbers in the literature.[54] Most likely, the electrical and optical properties of several zinc oxides with band gap energies (Eg) ranging from 2.100 to 3.760 eV were investigated previously for specific applications, such as photocatalysis.[55]

3.9. TON (Turnover Number) and TOF (Turnover Frequency). The efficacy and endurance of catalysts, such as zinc oxide nanoparticles, in the photocatalytic breakdown of dyes are assessed using two crucial parameters: turnover number (TON) and turnover frequency (TOF).

3.9.1. Turnover Number (TON). The efficacy of the catalyst (zinc oxide nanoparticles) was measured in dye degradation through turnover number.[56] The number of moles of degraded dye per catalyst molecule throughout the reaction is commonly estimated using the turnover number (TON).

$$\text{TON} = \frac{\text{number of moles of degraded dye}}{\text{number of moles of catalyst}}$$

https://doi.org/10.1021/acsomega.4c10628
ACS Omega 2025, 10, 7181−7193

According to the results of the treatment with zinc oxide nanoparticles, methylene blue and methyl orange dyes were destroyed by 94.45 and 85.99%, respectively. Based on degradation and catalyst, the turnover numbers of methylene blue and methyl orange were 0.048 and 0.041.

3.9.2. Turnover Frequency (TOF). The reaction rate is often studied by counting the number of reaction cycles that occur in a specific amount of time.[57]

$$\mathrm{TOF} = \frac{\mathrm{TON}}{\mathrm{time}}$$

Based on the degradation in the particular time period, the turnover frequency was calculated. The turnover frequencies of methylene blue and methyl orange were 4.44×10^{-6} and 4.56×10^{-6} s^{-1}. The TON and TOF values have demonstrated the effective photocatalytic activity of biosynthesized zinc oxide nanoparticles. TON and TOF values are performed by the catalyst, but there is some variance from previous results due to different experimental setups.[58,59]

3.10. Seed Germination Test. The process of priming involves pretreating seeds with certain solutions to improve germination and seedling development. Different treatments (50, 100, 150, and 200 ppm) of zinc oxide nanoparticles were used to assess pearl millet seed germination, root length, and shoot length (Table 3).

Table 3. Effects on Pearl Millet Seed Germination, Shoot Length, and Root Length of Varying Concentrations of Plant-Mediated Zinc Oxide Nanoparticles[a]

treatments	% germination	shoot length (cm)	root length (cm)
control	71.88 ± 1.34[a]	4.43 ± 0.20[a]	11.63 ± 0.41[a]
50 ppm	77.22 ± 2.52[b]	4.83 ± 0.15[a]	13.03 ± 0.68[b]
100 ppm	85.44 ± 3.24[c]	4.90 ± 0.10[a]	13.26 ± 0.32[b]
150 ppm	90.55 ± 1.38[d]	5.46 ± 0.25[b]	15.13 ± 0.35[c]
200 ppm	83.99 ± 3.21[c]	4.84 ± 0.32[a]	13.50 ± 0.36[b]

[a]Duncan's test shows that there is a significant difference ($P < 0.05$) between means ± SD shown in the column with the same letter. The variation in treatment is implied by the use of several letters.

Pearl millet primed seeds demonstrated higher root length, shoot length, and germination % at 150 ppm zinc oxide NP concentration. In comparison to the controlled treatment, the % seed germination was around 90.55%, the shoot length was 5.46 cm, and the root length was 15.13 cm at 150 ppm concentration (Table 3). A related study found that seed priming at 150 ppm zinc oxide nanoparticles increased the vigor index by 51% and the germination rate of pearl millet seeds by 20% in comparison to control (without treated).[48] Pearl millet seed germination and other physiological features were also studied using dyes (MB and MO) to determine how they affect pearl millet seeds.

MO- and MB-dye-treated pearl millet (*Pennisetum glaucum*) seedlings showed effects on seed germination and physiological reactions (Figure 10).

Pearl millet seeds were treated with MO and MB at various concentrations (0.5, 1.0, 1.5, and 2.0%). In the case of MO-treated seeds (2.0%), the germination % (15%), shoot length (5.13 cm), and root length (9.47 cm) were decreased compared with the control. Whereas, in MB-treated seeds at 2.0% concentration, the germination % (46%), shoot length (6.9 cm), and root length (10.4 cm) (Table 4).

A common basic dye used in biological staining techniques is methylene blue. Additionally, it may be harmful to plants, particularly in higher doses (2%). High levels of methylene blue, such as methyl orange, can harm seeds or interfere with cellular functions to prevent seed germination. Exposure to methylene blue and methyl orange can also have an effect on root growth and shoot length. But lower concentrations (0.5%) of both dyes have fewer effects on plant growth and seed germination %. In past reports, the toxic effects of various dyes were reported on wheat,[9] lettuce, wheat, and tomato seeds on plant growth and seed germination.[63] MB and MO are used in a variety of industries because of their varied qualities. However, because of their possible toxicity and negative effects on the environment and plant growth, their usage needs to be strictly regulated. These dyes most likely have an impact on germination-related enzymes.

3.11. Enzymes Involved in Seed Germination. In pearl millet seed germination, it involves different types of biochemical reactions catalyzed by various enzymes. Protein, lipid, and starch-containing spare food material in seeds are soluble in the actions of enzymes, including lipase, amylase, and protease. These enzymes also provide essential nutrients and energy to developing embryos (Figure 11).[64,65]

MB dye is more toxic than MO, but both synthetic dyes can inhibit seed germination. The inhibition of seedling growth and seed germination may vary with concentrations of dyes. Inhibition of seed germination by MB and MO can involve a combination of factors: change in pH, toxicity, and cellular damage. It was discovered that the textile dyes had a negative impact on the germination of pea, gram, and lentil seeds.[66] In our conducted experiment, both dyes (MO and MB) were shown to be toxic due to pearl millet seed germination and plant growth were affected (Table 4). These issues were

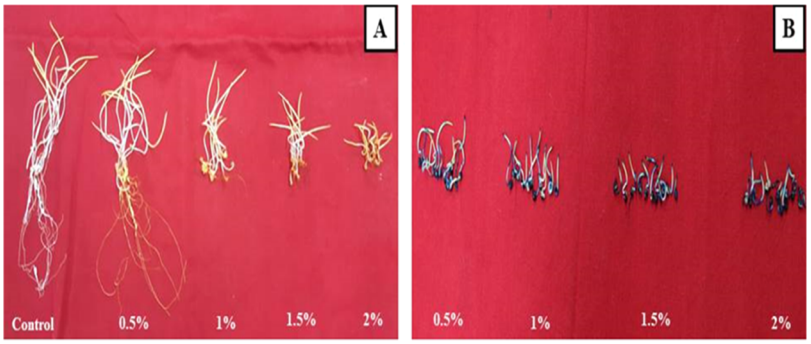

Figure 10. Pearl millet seedlings treated with (A) methyl orange (MO) and (B) methylene blue (MB).

https://doi.org/10.1021/acsomega.4c10628
ACS Omega 2025, 10, 7181−7193

Table 4. Effect of MO and MB Dyes on Pearl Millet % Seed Germination, Shoot Length, and Root Length[a]

	seed germination %		shoot length (cm)		root length (cm)	
treatments	MO	MB	MO	MB	MO	MB
control	74.66 ± 2.08[a]	74.66 ± 2.08[a]	8.01 ± 0.89[a]	8.01 ± 0.89[a]	10.79 ± 2.74[a]	10.79 ± 2.74[a]
0.5%	74.33 ± 2.88[a]	73.33 ± 4.16[a]	7.93 ± 0.70[a]	2.76 ± 0.38[b]	10.13 ± 2.21[a]	0.99 ± 0.42[b]
1.0%	71.66 ± 3.05[b]	65.00 ± 4.00[b]	5.20 ± 1.88[b]	1.65 ± 0.26[b]	2.75 ± 1.83[b]	0.61 ± 0.24[b]
1.5%	70.00 ± 3.60[b]	41.00 ± 2.64[c]	4.75 ± 0.67[b]	1.24 ± 0.39[b]	1.44 ± 0.49[b]	0.44 ± 0.24[b]
2.0%	59.66 ± 5.50[c]	28.66 ± 3.05[d]	2.88 ± 0.51[c]	1.11 ± 0.38[b]	1.32 ± 0.24[b]	0.39 ± 0.11[b]

[a]Duncan's test ($P \leq 0.05$) was used to determine the statistical significance. The resulting data were mentioned as mean values together with the relevant standard deviation (SD). The usage of multiple letters suggests substantial treatment variation.

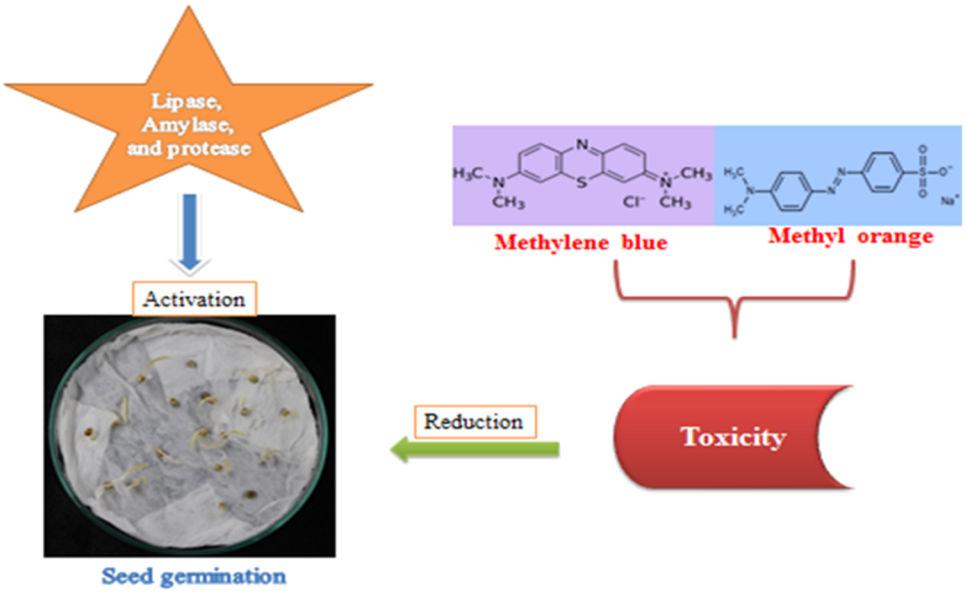

Figure 11. Various enzymes are involved in activation, whereas MO and MB dyes cause a reduction in pearl millet seed germination.

resolved using zinc nanoparticles to break down these dyes (MB and MO).

3.12. Photocatalytic Degradation. The process of breaking down a chemical into simpler, less hazardous compounds with the help of light and a photocatalyst is known as photocatalytic degradation (Figure 12). This method is frequently used for water purification, environmental cleanup, and the breakdown of contaminants in air and water.

Electrocatalysis and photocatalysis are two examples of advanced oxidation processes in which zinc nanoparticles can function as catalysts. Under UV light conditions, the dye solution (MB or MO) was mixed with zinc oxide nanoparticles, which act as photocatalysts. The excited zinc oxide nanoparticles produce ROS (reactive oxygen species) such as hydroxyl radicals (•OH) and superoxide radicals ($O_2^{\bullet -}$) when they are exposed to oxygen and water. The mechanism of photocatalytic degradation was followed by different equations.

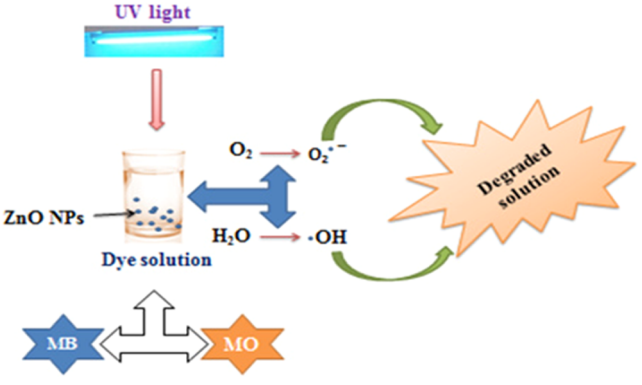

Figure 12. Mechanism of MO/MB dye degradation using zinc oxide nanoparticles under UV light conditions.

$$ZnO + h\nu \rightarrow ZnO + e^{-}(CB) + h^{+}(VB) \quad (7)$$

$$h^{+}(VB) + H_2O \rightarrow OH^{\bullet} + H^{+} \quad (8)$$

$$h^{+} + OH^{-} \rightarrow OH^{\bullet} \quad (9)$$

Electrons in the valence band (VB) of zinc oxide are stimulated into the conduction band (CB) when the valence band is stimulated by light energy that is greater than the band gap of zinc oxide.[67] The oxygenation of the water molecules and surface hydroxyl groups rapidly converted to a hydroxyl radical (eqs 8 and 9).

$$e^{-}(CB) + O_2 \rightarrow O_2^{\bullet -} \quad (10)$$

$$\text{dye} + \text{ROS} \rightarrow CO_2 + H_2O + \text{inorganic ions} \quad (11)$$

Superoxide radicals were produced when dissolved oxygen reacted with the electron conduction band (eq 10). Various types of ROS, such as hydroxyl radicals and superoxide anions, target and degrade dye (MB and MO) molecules in the form of carbon dioxide, water molecules, and inorganic ions (eq 11).[58,68,69] Because of the higher reactivity of ROS, it degrades dye into simpler molecules or less harmful compounds

https://doi.org/10.1021/acsomega.4c10628
ACS Omega 2025, 10, 7181−7193

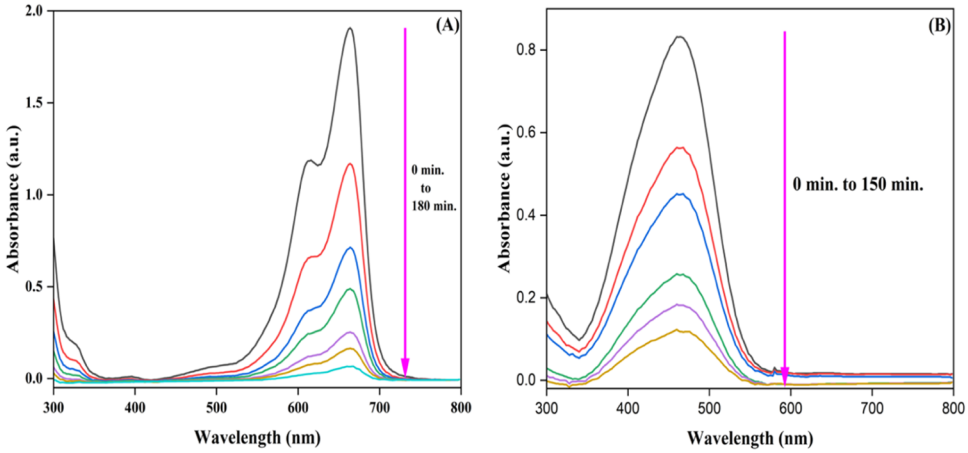

Figure 13. UV−visible spectra of (A) methylene blue and (B) methyl orange, showing photocatalytic degradation at different time intervals.

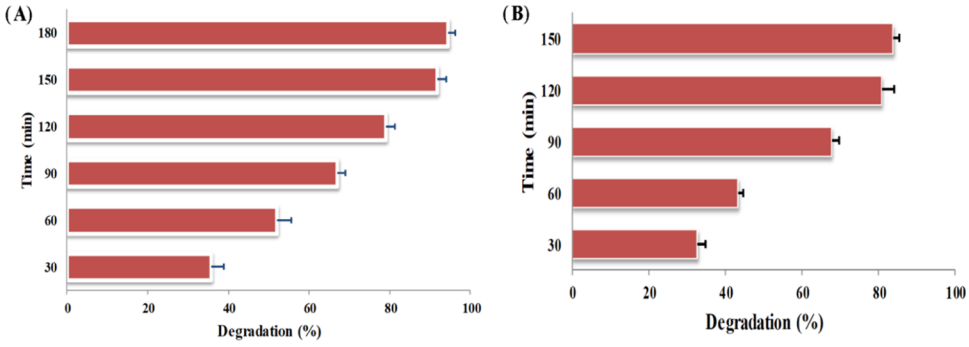

Figure 14. Degradation % of (A) MB and (B) MO with respect to time by biosynthesized zinc oxide nanoparticles.

(organic pollutants).[70] The UV−visible spectrum showed the degradation % of MB and MO at various time periods (Figure 13).

3.12.1. Methylene Blue. Nanoparticles are widely used in the efficient photocatalytic destruction of methylene blue. Owing to its wide band gap semiconductor and strong photocatalytic capabilities, zinc oxide nanoparticles can be used to degrade organic contaminants when exposed to UV or visible light (Figure 14).

The degradation of MB was noticed at various time periods (30, 60, 90, 120,150, and 180 min.). After 30, 60, 90, 120, 150, and 180 min, the average degradation percentage of MB had shown 35.67, 51.98, 67.00, 78.98, 91.76, and 94.45 (Figure 14). The result showed a higher degradation % of MB at 180 min. The average percentages of MB degradation at various time intervals show that degradation increases gradually with time. This pattern implies that the rate of degradation is time-dependent. The finding that the MB deterioration % exhibits approximately similar at both the 150 and 180 min periods and stays comparatively steady is particularly noteworthy. This plateauing effect raises the possibility that the equilibrium of deterioration may have reached a point beyond which more degradation is constrained. Additionally, a number of reports are in support, where MB dye % deteriorated at a higher level after treated zinc oxide nanoparticles.[71,72] Besides, Ag NPs showed photocatalytic prospective degrading methylene blue dye with an efficiency of 79% in 80 min, while EDLE@Au nanoparticles showed enhanced photocatalytic activity with 96.5% destruction.[43,73]

3.12.2. Methyl Orange. When zinc oxide nanoparticles are exposed to light, their breakdown usually results in the production of ROS, such as superoxide radicals ($O_2\bullet^-$) and hydroxyl radicals (•OH). These highly unstable ROS has the ability to oxidize MO. The photocatalytic (PC) activity of zinc oxide nanoparticles was tested against MO with respect to time (Figure 14).

The average degradation efficiencies were found to be 32.78, 45.39, 69.78, 78.90, and 85.99% after various time periods of 30, 60, 90, 120, and 150 min. The best result was found at 150 min after exposure to UV light, that was 85.99%. After 150 min, the degradation potential was not found for MO. The findings demonstrate how well UV light degrades MO, with the best degradation occurring after 150 min of exposure (Figure 13). Subsequent research endeavors might look into the fundamental mechanisms accountable for the noted degradation kinetics and examine approaches that address possible obstacles in accomplishing the total breakdown of MO. Zinc oxide nanoparticles have been used in a number of investigations to photocatalytically degrade methyl orange (MO), with differing degrees of efficiency reported depending on the characteristics of the nanoparticles, the production techniques, and the reaction circumstances.[25,74] Due to catalyst activation and the production of reactive species, methyl orange (MO) demonstrated 85% photodegradation in 120 min when exposed to sunlight.[20] There were further reports of dye degradation that were compared with the present study (Table 5).

3.13. Antioxidant Assay. The antioxidant assay was performed to scavenge free radicals through biosynthesized

https://doi.org/10.1021/acsomega.4c10628
ACS Omega 2025, 10, 7181−7193

Table 5. Comparison Table of Photodegradation Efficiency of Synthesized Zinc Oxide Nanoparticles

photocatalyst	dyes	degradation (%)	time (min)	ref.
zinc oxide	MB	37	120	75
biosynthesized zinc oxide	MO	84	120	25
biosynthesized zinc oxide	MB and MO	75 and 87	180	39
biosynthesized zinc oxide	MB and MO	84 and 88	60 and 150	76
biosynthesized zinc oxide	MB and MO	94 and 85	180 and 150	present work

zinc oxide nanoparticles. The solution containing zinc oxide nanoparticles and DPPH exhibited a gradual color change in the dark. Nanoparticles can donate the electron to the DPPH free radicals and neutralize it (Figure 15).

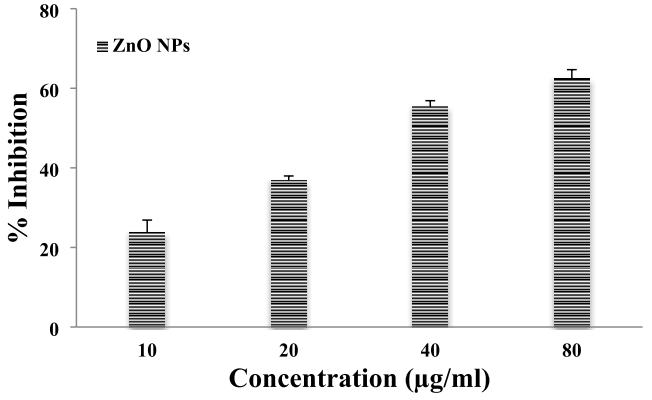

Figure 15. Inhibition (%) of DPPH through zinc oxide nanoparticles at different concentrations.

The % inhibition rose as the concentration of zinc oxide nanoparticles increased, indicating that the antioxidant action of Zn nanoparticles was dose-dependent. The maximum inhibition % was recorded as 62.39 at 80 μg/mL concentration. Our findings are supported by numerous published research that demonstrate the antioxidant activity varied at different doses.[77−79] zinc oxide nanoparticles demonstrated antibacterial action in addition to their excellent antioxidant capacity.

3.14. Antibacterial Assay. Zinc nanoparticles at varying concentrations were tested for their antibacterial activity against *E. coli* and *S. aureus* bacteria. In *E. coli*, the zone of inhibition was detected to be 0.2, 0.35, and 0.45 cm at concentrations of 10, 50, and 100 mg/mL, respectively (Figure 16).

In contrast, at concentrations of 1 and 10 mg/mL, no inhibitory zone was seen for *S. aureus*. Whereas, the zone of inhibition was detected to be 0.25 and 0.35 cm at concentrations of 50 and 100 mg/mL (Figure 16). The minimum inhibitory concentration (MIC) of zinc nanoparticles against *E. coli* and *S. aureus* was determined to be 10 and 50 mg/mL, respectively. The antibacterial effectiveness of zinc oxide nanoparticles against *S. aureus* and *E. coli* at varying doses has been assessed in recent reports.[80,81]

4. CONCLUSIONS

Biosynthesized zinc oxide nanoparticles exhibited a number of encouraging properties, such as crystalline structure and photocatalytic activity. MB and MO showed toxicity effects on seedling growth and seed germination (46 and 15%) on pearl millet, whereas the MB dye was more toxic than MO. Various industries released such dyes, which polluted the environment. Zinc oxide nanoparticles have a higher proportion of seed germination (a concentration of 150 ppm) and the capacity to degrade MB (94.45%) and MO (85.99%) dyes. It also demonstrated high antibacterial activity against *E. coli* and *S. aureus* (100 mg/mL). Additionally, the zinc oxide nanoparticles have high antioxidant activity recorded at 80 μg/mL. The future aspects of this research may lead to fully realize the potential benefits for society, particularly in the areas of wastewater treatment (due to dye degradation), agriculture (due to improved seed germination), biological sciences (due to antioxidant activity), and application in food science (due to antibacterial activity). Safety and sustainable ZnO NP manufacturing and usage should also be prioritized to reduce environmental and health risks.

AUTHOR INFORMATION

Corresponding Author

Madan Mohan Sharma − *Department of Biosciences, Manipal University Jaipur, Jaipur 303007 Rajasthan, India;* orcid.org/0000-0002-8615-7177; Email: madanmohan.sharma@jaipur.manipal.edu

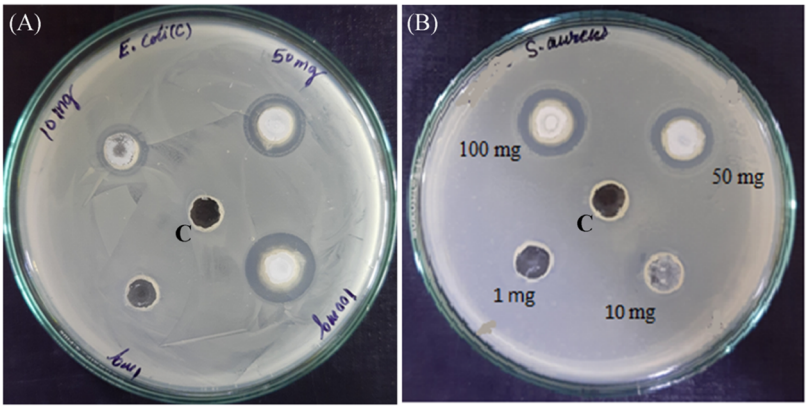

Figure 16. Antibacterial activity of biosynthesized zinc oxide nanoparticles against (A) *E. coli*, and (B) *S. aureus* at different concentrations.

https://doi.org/10.1021/acsomega.4c10628
ACS Omega 2025, 10, 7181−7193

Authors

Rajesh Kumar − *Department of Biosciences, Manipal University Jaipur, Jaipur 303007 Rajasthan, India*

Irra Dhar − *Department of Biosciences, Manipal University Jaipur, Jaipur 303007 Rajasthan, India*

Complete contact information is available at: https://pubs.acs.org/10.1021/acsomega.4c10628

Author Contributions

R.K.: conceptualization, original draft; I.D.: writing—review and editing; M.M.S.: conceptualization, methodology, validation, supervision.

Funding

Financial support in the form of the DST-FIST project (DST/2022/1012) from the Government of India is gratefully acknowledged.

Notes

The authors declare no competing financial interest.

■ ACKNOWLEDGMENTS

The authors acknowledge the support of Central Analytical Facilities and Sophisticated Analytical Instrument Facilities in Manipal University Jaipur for characterization works.

■ REFERENCES

(1) Altieri, M.; Nicholls, C. I. *Sustainable Agriculture Reviews*; Wiley, 2012; Vol. *11*.

(2) Kaur, A.; Vats, S.; Rekhi, S.; Bhardwaj, A.; Goel, J.; Goel, J.; Tanwar, R. S.; Tanwar, R. S.; Gaur, K. K. Physico-Chemical Analysis of the Industrial Effluents and Their Impact on the Soil Microflora. *Procedia Environ. Sci.* **2010**, *2*, 595−599.

(3) Banat, I. M.; Nigam, P.; Singh, D.; Marchant, R. Microbial Decolorization of Textile-Dye-Containing Effluents: A Review. *Bioresour. Technol.* **1996**, *58* (3), 217−227.

(4) Michaels, G. B.; Lewis, D. L. Sorption and Toxicity of Azo and Triphenylmethane Dyes To Aquatic Microbial Populations. *Environ. Toxicol. Chem.* **1985**, *4* (1), 45.

(5) Topaç, F. O.; Dindar, E.; Uçaroğlu, S.; Başkaya, H. S. Effect of a Sulfonated Azo Dye and Sulfanilic Acid on Nitrogen Transformation Processes in Soil. *J. Hazard. Mater.* **2009**, *170* (2−3), 1006−1013.

(6) Kasthuri, R.; Kalaivani, D.; Banumathi, K.; Shanmugapriya, R. Evaluation of Water Quality in A. Mettur Area of Perambalur District. *Indian J. Environ. Prot.* **2007**, *1*, 1011−1014.

(7) Patel, H.; et al. Physico-chemical Characterisation Of Textile Chemical Sludge Physico-chemical Characterisation Of Textile Chemical Sludge Generated From Various Key Words: Textile Industry; Chemical Sludge, Characterisation, Waste Management. *Energy* **2008**, *2*, 329−339.

(8) Naik, D. J.; Desai, K. K.; Vashi, R. T. Physico-Chemical Characteristics of Chemical Sludge Generated from Treatment of Combined Wastewater of Dyes and Dye Intermediate Manufacturing Industries. *J. Environ. Res. Dev.* **2009**, *4* (2), 413−416.

(9) Haque, M. M.; Haque, M. A.; Mosharaf, M. K.; Marcus, P. K. Decolorization, Degradation and Detoxification of Carcinogenic Sulfonated Azo Dye Methyl Orange by Newly Developed Biofilm Consortia. *Saudi J. Biol. Sci.* **2021**, *28* (1), 793−804.

(10) Dutta, S. K.; Elias, M.; Anis-Ul-Haque, K. M.; Dhar, P. K.; Mizanur, M.; Khan, R.; Amin, K. Cost-Effective and Eco-Friendly Leaf-Based Bio-Adsorbent for Methyl Blue Dye Adsorption: Thermodynamics, Kinetics, Isotherms, and Phytotoxicity, 2023. https://doi.org/10.21203/rs.3.rs-2432305/v1.

(11) Hassan, J.; Zia, M.; Kamal, U.; Alam, M. Z. Impact of Textile Dyeing Effluents on Germination and Seedling Stage of Coutnry Bean (Lablab Niger Var. Typicus) Eclectic Conductivity. *Environ. Nat. Resour. J.* **2013**, *11* (2), 80−96.

(12) Rajan, D. N. S. Phytotoxic Effect of Dyeing Industry Effluent on Seed Germination and Early Growth of Lady?S Finger. *J. Pollut. Eff. Control* **2015**, *03* (02), 2−5.

(13) Rahman, M.; Rayhan, M.; Chowdhury, M.; Mohiuddin, K.; Chowdhury, M. Phytotoxic Effect of Synthetic Dye Effluents on Seed Germination and Early Growth of Red Amaranth. *Fundam. Appl. Agric.* **2019**, *4* (1), 480.

(14) Nath, K.; Singh, D.; Sharma, Y. K. Combinatorial Effects of Distillery and Sugar Factory Effluents in Crop Plants. *J. Environ. Biol.* **2007**, *28* (3), 577−582.

(15) Auld, D. S. Zinc Coordination Sphere in Biochemical Zinc Sites. *BioMetals* **2001**, *14* (3−4), 271−313.

(16) Jones, N.; Ray, B.; Ranjit, K. T.; Manna, A. C. Antibacterial Activity of Zinc oxide Nanoparticle Suspensions on a Broad Spectrum of Microorganisms. *FEMS Microbiol. Lett.* **2008**, *279* (1), 71−76.

(17) Singh, J.; Dutta, T.; Kim, K. H.; Rawat, M.; Samddar, P.; Kumar, P. Green" Synthesis of Metals and Their Oxide Nanoparticles: Applications for Environmental Remediation. *J. Nanobiotechnol.* **2018**, *16* (1), 84.

(18) Singh, J.; Kumar, S.; Alok, A.; Upadhyay, S. K.; Rawat, M.; Tsang, D. C. W.; Bolan, N.; Kim, K. H. The Potential of Green Synthesized Zinc Oxide Nanoparticles as Nutrient Source for Plant Growth. *J. Cleaner Prod.* **2019**, *214*, 1061−1070.

(19) Ullah, S.; Shaban, M.; Siddique, A. B.; Zulfiqar, A.; Lali, N. S.; Naeem-ul-Hassan, M.; Irfan, M. I.; Sher, M.; Fayyaz ur Rehman, M.; Hanbashi, A.; Sabei, F. Y.; Amin, H. M. A.; Abbas, A. Greenly Synthesized Zinc Oxide Nanoparticles: An Efficient, Cost-Effective Catalyst for Dehydrogenation of Formic Acid and with Improved Antioxidant and Phyto-Toxic Properties. *J. Environ. Chem. Eng.* **2024**, *12* (5), No. 113350.

(20) Siddique, A. B.; Shaheen, M. A.; Abbas, A.; Zaman, Y.; Ali, A.; Naeem-ul-Hassan, M.; Iqbal, J. Photocatalytic and Biological Efficacy of Carissa Macrocarpa Fruit Extract-Mediated One-Pot Synthesized Ternary Metal Oxide Dual S-Scheme Heterojunction. *J. Environ. Chem. Eng.* **2024**, *12* (3), No. 112725.

(21) Ejaz, A.; Mamtaz, Z.; Yasmin, I.; Shaban, M.; Siddique, A. B.; Irfan, M. I.; Ali, A.; Muhammad, S.; Sameeh, M. Y.; Abbas, A. Cyperus Scariosus Extract Based Greenly Synthesized Gold Nanoparticles as Colorimetric Nanoprobe for Ni2+ Detection and as Antibacterial and Photocatalytic Agent. *J. Mol. Liq.* **2024**, *393*, No. 123622.

(22) Shah, A.; Akhtar, S.; Mahmood, F.; Urooj, S.; Siddique, A. B.; Irfan, M. I.; Naeem-ul-Hassan, M.; Sher, M.; Alhoshani, A.; Rauf, A.; Amin, H. M. A.; Abbas, A. Fagonia Arabica Extract-Stabilized Gold Nanoparticles as a Highly Selective Colorimetric Nanoprobe for Cd2+ Detection and as a Potential Photocatalytic and Antibacterial Agent. *Surf. Interfaces* **2024**, *51*, No. 104556.

(23) Pirhashemi, M.; Habibi-Yangjeh, A.; Rahim Pouran, S. Review on the Criteria Anticipated for the Fabrication of Highly Efficient Zinc oxide-Based Visible-Light-Driven Photocatalysts. *J. Ind. Eng. Chem.* **2018**, *62*, 1−25.

(24) Abada, B.; Alivio, T. E. G.; Shao, Y.; O'Loughlin, T. E.; Klemashevich, C.; Banerjee, S.; Jayaraman, A.; Chu, K. H. Photodegradation of Fluorotelomer Carboxylic 5:3 Acid and Perfluorooctanoic Acid Using Zinc Oxide. *Environ. Pollut.* **2018**, *243*, 637−644.

(25) Karnan, T.; Selvakumar, S. A. S. *Biosynthesis of Zinc oxide Nanoparticles Using Rambutan (Nephelium Lappaceum L.) Peel Extract and Their Photocatalytic Activity on Methyl Orange Dye*; Elsevier Ltd., 2016; Vol. *1125*.

(26) Ravichandran, V.; Sumitha, S.; Ning, C. Y.; Xian, O. Y.; Kiew Yu, U.; Paliwal, N.; Shah, S. A. A.; Tripathy, M. Durian Waste Mediated Green Synthesis of Zinc Oxide Nanoparticles and Evaluation of Their Antibacterial, Antioxidant, Cytotoxicity and Photocatalytic Activity. *Green Chem. Lett. Rev.* **2020**, *13* (2), 102−116.

(27) Yadav, R. S.; Mishra, P.; Pandey, A. C. Growth Mechanism and Optical Property of Zinc oxide Nanoparticles Synthesized by Sonochemical Method. *Ultrason. Sonochem.* **2008**, *15* (5), 863−868.

(28) Chen, D.; Wang, Z.; Ren, T.; Ding, H.; Yao, W.; Zong, R.; Zhu, Y. Influence of Defects on the Photocatalytic Activity of Zinc oxide. *J. Phys. Chem. C* **2014**, *118* (28), 15300−15307.
(29) Manjunath, K.; Ravishankar, T. N.; Kumar, D.; Priyanka, K. P.; Varghese, T.; Naika, H. R.; Nagabhushana, H.; Sharma, S. C.; Dupont, J.; Ramakrishnappa, T.; Nagaraju, G. Facile Combustion Synthesis of Zinc oxide Nanoparticles Using Cajanus Cajan (L.) and Its Multidisciplinary Applications. *Mater. Res. Bull.* **2014**, *57*, 325−334.
(30) Brand-Williams, W.; Cuvelier, M. E.; Berset, C. Use of a Free Radical Method to Evaluate Antioxidant Activity. *LWT − Food Sci. Technol.* **1995**, *28* (1), 25−30.
(31) Elumalai, K.; Velmurugan, S.; Ravi, S.; Kathiravan, V.; Ashokkumar, S. Bio-Fabrication of Zinc Oxide Nanoparticles Using Leaf Extract of Curry Leaf (Murraya Koenigii) and Its Antimicrobial Activities. *Mater. Sci. Semicond. Process.* **2015**, *34*, 365−372.
(32) Thakral, F.; Bhatia, G. K.; Tuli, H. S.; Sharma, A. K.; Sood, S. Zinc Oxide Nanoparticles: From Biosynthesis, Characterization, and Optimization to Synergistic Antibacterial Potential. *Curr. Pharmacol. Reports* **2021**, *7* (1), 15−25.
(33) Happy, A.; Soumya, M.; Venkat Kumar, S.; Rajeshkumar, S.; Sheba Rani, N. D.; Lakshmi, T.; Deepak Nallaswamy, V. Phyto-Assisted Synthesis of Zinc Oxide Nanoparticles Using Cassia Alata and Its Antibacterial Activity against *Escherichia Coli*. *Biochem. Biophys. Rep.* **2019**, *17*, 208−211.
(34) Hasanin, M.; Hassan, S. A. M.; Hosny, A. Green Biosynthesis of Zinc and Selenium Oxide Nanoparticles Using Callus Extract of Ziziphus Spina - Christi: Characterization, Antimicrobial, and Antioxidant Activity. *Biomass Convers. Bioref.* **2021**, *13*, 10133−10146.
(35) Awan, S.; Shahzadi, K.; Javad, S.; Tariq, A.; Ahmad, A.; Ilyas, S. A Preliminary Study of Influence of Zinc Oxide Nanoparticles on Growth Parameters of Brassica Oleracea Var Italic. *J. Saudi Soc. Agric. Sci.* **2021**, *20* (1), 18−24.
(36) Kamble, V. V.; Gaikwad, N. Fourier Transform Infrared Spectroscopy Spectroscopic Studies in Embelia Ribes Burm, 2016.
(37) Moussi, A.; Mahiou, L. Electroless Plating, a Simple Route for Nickel Deposition for Solar Cells, 2016.
(38) Jabbar, A.; Abbas, A.; Assad, N.; Naeem-Ul-Hassan, M.; Alhazmi, H. A.; Najmi, A.; Zoghebi, K.; Al Bratty, M.; Hanbashi, A.; Amin, H. M. A. A Highly Selective Hg2+ Colorimetric Sensor and Antimicrobial Agent Based on Green Synthesized Silver Nanoparticles Using Equisetum Diffusum Extract. *RSC Adv.* **2023**, *13* (41), 28666−28675.
(39) Ghaffar, S.; Abbas, A.; Naeem-ul-Hassan, M.; Assad, N.; Sher, M.; Ullah, S.; Alhazmi, H. A.; Najmi, A.; Zoghebi, K.; Al Bratty, M.; Hanbashi, A.; Makeen, H. A.; Amin, H. M. A. Improved Photocatalytic and Antioxidant Activity of Olive Fruit Extract-Mediated Zinc oxide Nanoparticles. *Antioxidants* **2023**, *12* (6), No. 1201, DOI: 10.3390/antiox12061201.
(40) Yedurkar, S.; Maurya, C.; Mahanwar, P. Biosynthesis of Zinc Oxide Nanoparticles Using Ixora Coccinea Leaf Extract—A Green Approach. *Open J. Synth. Theory Appl.* **2016**, *05* (01), 1−14.
(41) Yusof, N. A. A.; Zain, N. M.; Pauzi, N. Synthesis of Zinc oxide Nanoparticles with Chitosan as Stabilizing Agent and Their Antibacterial Properties against Gram-Positive and Gram-Negative Bacteria. *Int. J. Biol. Macromol.* **2019**, *124*, 1132−1136.
(42) Zarei, M. FTIR Spectroscopic Studies On Cleome Gynandra − Comparative, 2013.
(43) Khan, A. W.; Lali, N. S.; Sabei, F. Y.; Irfan, M. I.; Naeem-ul-Hassan, M.; Sher, M.; Safhi, A. Y.; Alsalhi, A.; Albariqi, A. H.; Kamli, F.; Amin, H. M. A.; Abbas, A. Sunlight-Assisted Green Synthesis of Gold Nanocubes Using Horsetail Leaf Extract: A Highly Selective Colorimetric Sensor for Pb2+, Photocatalytic and Antimicrobial Agent. *J. Environ. Chem. Eng.* **2024**, *12* (3), No. 112576.
(44) Assad, N.; Naeem-ul-Hassan, M.; Ajaz Hussain, M.; Abbas, A.; Sher, M.; Muhammad, G.; Assad, Y.; Farid-ul-Haq, M. Diffused Sunlight Assisted Green Synthesis of Silver Nanoparticles Using Cotoneaster Nummularia Polar Extract for Antimicrobial and Wound Healing Applications. *Nat. Prod. Res.* **2023**, DOI: 10.1080/14786419.2023.2295936.
(45) Abeysinghe, D. T.; Kumara, K. A. H.; Kaushalya, K. A. D.; Chandrika, U. G.; Alwis, D. D. D. H. Phytochemical Screening, Total Polyphenol, Flavonoid Content, in Vitro Antioxidant and Antibacterial Activities of Sri Lankan Varieties of Murraya Koenigii and Micromelum Minutum Leaves. *Heliyon* **2021**, *7* (7), No. e07449.
(46) Igara, C.; Omoboyowa, D.; Ahuchaogu, A.; Orji, N.; Ndukwe, M. Phytochemical and Nutritional Profile of Murraya Koenigii (Linn) Spreng Leaf CE Igara, DA Omoboyowa, AA Ahuchaogu, NU Orji and MK Ndukwe. *J. Pharmacogn. Phytochem.* **2016**, *5* (5), 4−7.
(47) Chaudhuri, S. K.; Malodia, L. Biosynthesis of Zinc Oxide Nanoparticles Using Leaf Extract of Calotropis Gigantea: Characterization and Its Evaluation on Tree Seedling Growth in Nursery Stage. *Appl. Nanosci.* **2017**, *7* (8), 501−512.
(48) Kumar, R.; Dadhich, A.; Dhiman, M.; Sharma, L.; Sharma, M. M. Stimulatory Effect of Zinc oxide Nanoparticles as a Nanofertilizer in Seed Priming of Pearl Millet (Pennisetum Glaucum) and Their Bioactivity Studies. *S. Afr. J. Bot.* **2024**, *165*, 30−38.
(49) Olechnowicz, J.; Tinkov, A.; Skalny, A.; Suliburska, J. Zinc Status Is Associated with Inflammation, Oxidative Stress, Lipid, and Glucose Metabolism. *J. Physiol. Sci.* **2018**, *68* (1), 19−31.
(50) Kavithaa, K.; Paulpandi, M.; Ponraj, T.; Murugan, K.; Sumathi, S. Induction of Intrinsic Apoptotic Pathway in Human Breast Cancer (MCF-7) Cells through Facile Biosynthesized Zinc Oxide Nanorods. *Karbala Int. J. Mod. Sci.* **2016**, *2* (1), 46−55.
(51) Elshayb, O. M.; Farroh, K. Y.; Amin, H. E.; Atta, A. M. Green Synthesis of Zinc Oxide Nanoparticles: Fortification for Rice Grain Yield and Nutrients Uptake Enhancement. *Molecules* **2021**, *26* (3), 584.
(52) El-Megharbel, S. M.; Alsawat, M.; Al-Salmi, F. A.; Hamza, R. Z. Utilizing of (Zinc Oxide Nano-Spray) for Disinfection against "Sars-Cov-2" and Testing Its Biological Effectiveness on Some Biochemical Parameters during (Covid-19 Pandemic)—"zinc oxide Nanoparticles Have Antiviral Activity against (Sars-Cov-2). *Coatings* **2021**, *11* (4), No. 388, DOI: 10.3390/coatings11040388.
(53) Jin, W.; Lee, I. K.; Kompch, A.; Dörfler, U.; Winterer, M. Chemical Vapor Synthesis and Characterization of Chromium Doped Zinc Oxide Nanoparticles. *J. Eur. Ceram. Soc.* **2007**, *27* (13−15), 4333−4337.
(54) El-Kemary, M.; El-Shamy, H.; El-Mehasseb, I. Photocatalytic Degradation of Ciprofloxacin Drug in Water Using Zinc oxide Nanoparticles. *J. Lumin.* **2010**, *130* (12), 2327−2331.
(55) Zhang, Y.; Xu, X. Machine Learning Optical Band Gaps of Doped-Zinc oxide Films. *Optik* **2020**, *217* (April), No. 164808.
(56) Boudart, M. Turnover Rates in Heterogeneous Catalysis. *Chem. Rev.* **1995**, *95* (3), 661−666.
(57) Devi, L. G.; Shyamala, R. Photocatalytic Activity of SnO2-a-Fe2O3 Composite Mixtures: Exploration of Number of Active Sites, Turnover Number and Turnover Frequency. *Mater. Chem. Front.* **2018**, *2* (4), 796−806.
(58) Siva, N.; Sakthi, D.; Ragupathy, S.; Arun, V.; Kannadasan, N. Synthesis, Structural, Optical and Photocatalytic Behavior of Sn Doped Zinc oxide Nanoparticles. *Mater. Sci. Eng. B* **2020**, *253*, No. 114497.
(59) Fatima, B.; Siddiqui, S. I.; Ahmad, R.; Linh, N. T. T.; Thai, V. N. CuO-Zinc oxide-CdWO4: A Sustainable and Environmentally Benign Photocatalytic System for Water Cleansing. *Environ. Sci. Pollut. Res.* **2021**, *28* (38), 53793−53803.
(60) Moharram, A. H.; Mansour, S. A.; Hussein, M. A.; Rashad, M. Direct Precipitation and Characterization of Zinc oxide Nanoparticles. *J. Nanomater.* **2014**, *2014*, No. 716210, DOI: 10.1155/2014/716210.
(61) Singh, A. K.; Viswanath, V.; Janu, V. C. Synthesis, Effect of Capping Agents, Structural, Optical and Photoluminescence Properties of Zinc oxide Nanoparticles. *J. Lumin.* **2009**, *129* (8), 874−878.
(62) Rami, J. M.; Patel, C. D.; Patel, C. M.; Patel, M. V. Thermogravimetric Analysis (TGA) of Some Synthesized Metal Oxide Nanoparticles. *Mater. Today Proc.* **2021**, *43*, 655−659.

(63) Moawad, H.; Abd El-Rahim, W. M.; Khalafallah, M. Evaluation of Biotoxicity of Textile Dyes Using Two Bioassays. *J. Basic Microbiol.* **2003**, *43* (3), 218−229.
(64) Joshi, R. Role of Enzymes in Seed Germination. *Int. J. Creat. Res. Thoughts* **2018**, *6* (2), 1481−1485.
(65) Kumar, R. R.; Bhargava, D. V.; Pandit, K.; Goswami, S.; Mukesh Shankar, S.; Singh, S. P.; Rai, G. K.; Tara Satyavathi, C.; Praveen, S. Lipase − The Fascinating Dynamics of Enzyme in Seed Storage and Germination − A Real Challenge to Pearl Millet. *Food Chem.* **2021**, *361*, No. 130031.
(66) Nasrin, T.; Saha, A. K.; Mohanta, M. K.; Saha, A.; Rahman, S. A.; Ruhi, R. A.; Sarker, S. R. Decolourization of Azo Dye by Indigenous Bacteria and Its Impact on Seed Germination. *Int. J. Biosci.* **2019**, *6655*, 197−210.
(67) Ibrahim, M. M. Photocatalytic Activity of Nanostructured Zinc oxide − ZrO2 Binary Oxide Using Fluorometric Method. *Spectrochim. Acta, Part A* **2015**, *145*, 487−492, DOI: 10.1016/j.saa.2015.02.057.
(68) Pal, U.; Mora, E. S. Photocatalytic Behavior of Zinc oxide and Pt-Incorporated Zinc oxide Nanoparticles in Phenol Degradation. *Appl. Catal., A* **2011**, *394* (1−2), 269−275.
(69) Ali, L. I.; El-molla, S. A.; Ibrahim, M. M.; Mahmoud, H. R.; Naghmash, M. A. Effect of Preparation Methods and Optical Band Gap of Zinc oxide Nanomaterials on Photodegradation Studies. *Opt. Mater.* **2016**, *58*, 484−490.
(70) Tahir, M. B.; Nabi, G.; Rafique, M.; Khalid, N. R. Nanostructured-Based WO3 Photocatalysts: Recent Development, Activity Enhancement, Perspectives and Applications for Wastewater Treatment. *Int. J. Environ. Sci. Technol.* **2017**, *14* (11), 2519−2542.
(71) Karkhane, M.; Lashgarian, H. E.; Mirzaei, S. Z.; Ghaffarizadeh, A.; cherghipour, K.; Sepahvand, A.; Marzban, A. Antifungal, Antioxidant and Photocatalytic Activities of Zinc Nanoparticles Synthesized by Sargassum Vulgare Extract. *Biocatal. Agric. Biotechnol.* **2020**, *29*, No. 101791.
(72) Bhatia, S.; Verma, N. Photocatalytic Activity of Zinc oxide Nanoparticles with Optimization of Defects. *Mater. Res. Bull.* **2017**, *95*, 468−476.
(73) Siddique, A. B.; Amr, D.; Abbas, A.; Zohra, L.; Irfan, M. I.; Alhoshani, A.; Ashraf, S.; Amin, H. M. A. Synthesis of Hydroxyethylcellulose Phthalate-Modified Silver Nanoparticles and Their Multifunctional Applications as an Efficient Antibacterial, Photocatalytic and Mercury-Selective Sensing Agent. *Int. J. Biol. Macromol.* **2024**, *256*, No. 128009, DOI: 10.1016/j.ijbiomac.2023.128009.
(74) Gawade, V. V.; Gavade, N. L.; Shinde, H. M.; Babar, S. B.; Kadam, A. N.; Garadkar, K. M. Green Synthesis of Zinc oxide Nanoparticles by Using Calotropis Procera Leaves for the Photodegradation of Methyl Orange. *J. Mater. Sci. Mater. Electron.* **2017**, *28* (18), 14033−14039.
(75) Azarang, M.; Shuhaimi, A.; Yousefi, R.; Jahromi, S. P. One-Pot Sol-Gel Synthesis of Reduced Graphene Oxide Uniformly Decorated Zinc Oxide Nanoparticles in Starch Environment for Highly Efficient Photodegradation of Methylene Blue. *RSC Adv.* **2015**, *5* (28), 21888−21896.
(76) Gawade, V. V.; Sabale, S. R.; Dhabbe, R. S.; Kite, S. V.; Garadkar, K. M. Bio-Mediated Synthesis of Zinc oxide Nanostructures for Efficient Photodegradation of Methyl Orange and Methylene Blue. *J. Mater. Sci. Mater. Electron.* **2021**, *32* (24), 28573−28586, DOI: 10.1007/s10854-021-07235-0.
(77) Mahendra, C.; Chandra, M. N.; Murali, M.; Abhilash, M. R.; Singh, S. B.; Satish, S.; Sudarshana, M. S. Phyto-Fabricated Zinc oxide Nanoparticles from Canthium Dicoccum (L.) for Antimicrobial, Anti-Tuberculosis and Antioxidant Activity. *Process Biochem.* **2020**, *89*, 220−226.
(78) Brindhadevi, K.; Samuel, M. S.; Verma, T. N.; Vasantharaj, S.; Sathiyavimal, S.; Saravanan, M.; Pugazhendhi, A.; Duc, P. A. Zinc Oxide Nanoparticles (Zinc oxideNPs) -Induced Antioxidants and Photocatalytic Degradation Activity from Hybrid Grape Pulp Extract (HGPE). *Biocatal. Agric. Biotechnol.* **2020**, *28*, No. 101730, DOI: 10.1016/j.bcab.2020.101730.
(79) Madan, H. R.; Sharma, S. C.; Udayabhanu; Suresh, D.; Vidya, Y. S.; Nagabhushana, H.; Rajanaik, H.; Anantharaju, K. S.; Prashantha, S. C.; Sadananda Maiya, P. Facile Green Fabrication of Nanostructure Zinc oxide Plates, Bullets, Flower, Prismatic Tip, Closed Pine Cone: Their Antibacterial, Antioxidant, Photoluminescent and Photocatalytic Properties. *Spectrochim. Acta, Part A* **2016**, *152*, 404−416.
(80) Elumalai, K.; Velmurugan, S. Green Synthesis, Characterization and Antimicrobial Activities of Zinc Oxide Nanoparticles from the Leaf Extract of Azadirachta Indica (L.). *Appl. Surf. Sci.* **2015**, *345*, 329−336.
(81) Lingaraju, K.; Raja Naika, H.; Manjunath, K.; Basavaraj, R. B.; Nagabhushana, H.; Nagaraju, G.; Suresh, D. Biogenic Synthesis of Zinc Oxide Nanoparticles Using Ruta Graveolens (L.) and Their Antibacterial and Antioxidant Activities. *Appl. Nanosci.* **2016**, *6* (5), 703−710.

https://doi.org/10.1021/acsomega.4c10628
ACS Omega 2025, 10, 7181−7193